Appendix A. Supplementary data

Supporting Information of Construction of Noble Metal-Loaded Functional catalysts for Highly Efficient Catalytic Dehydrogenation of Ammonia Borane via Hydrolysis

SEM and TEM were used to characterize the morphology and microstructure of materials. XRD was utilized to analyze the crystal structure, phase composition and physical properties of the materials. XPS was utilized to analyze the elemental composition, chemical state and structure of the material surface.

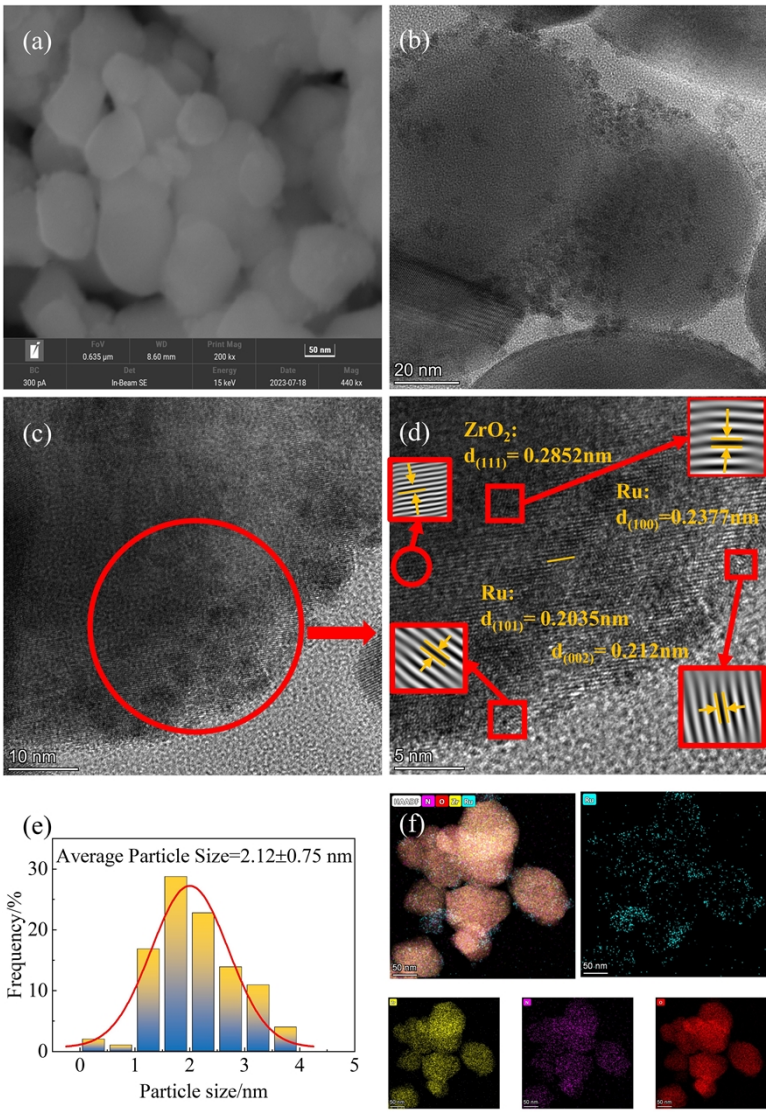

Fig.S1 The SEM (a)and TEM (b, c, d) images of 3%Ru/ZrO_2. (e) The corresponding histogram shows the particle size distribution (average particle size=2.12 nm). (f) The EDX elemental mapping images of 3%Ru/ZrO_2 with Ru (blue), N (purple) from residual N_2, Zr (yellow) and O (red).

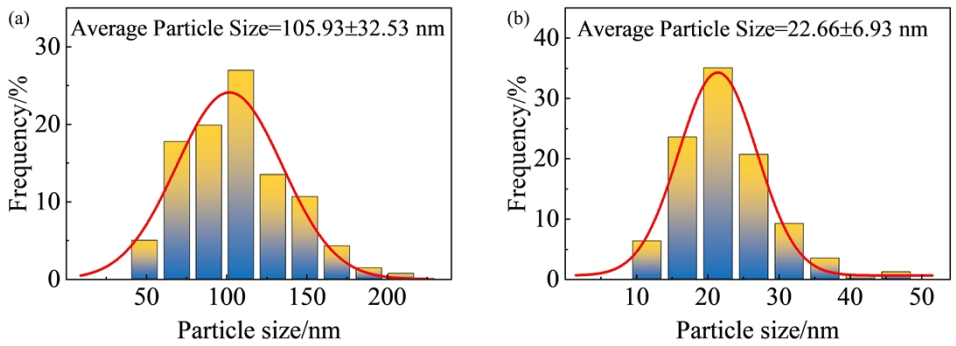

Fig.S2 The histogram graphs of the support particle size distribution: (a) ZrO_2 and (b) Zr_2ON_2.

The measured average particle size is displayed at the top of each panel.

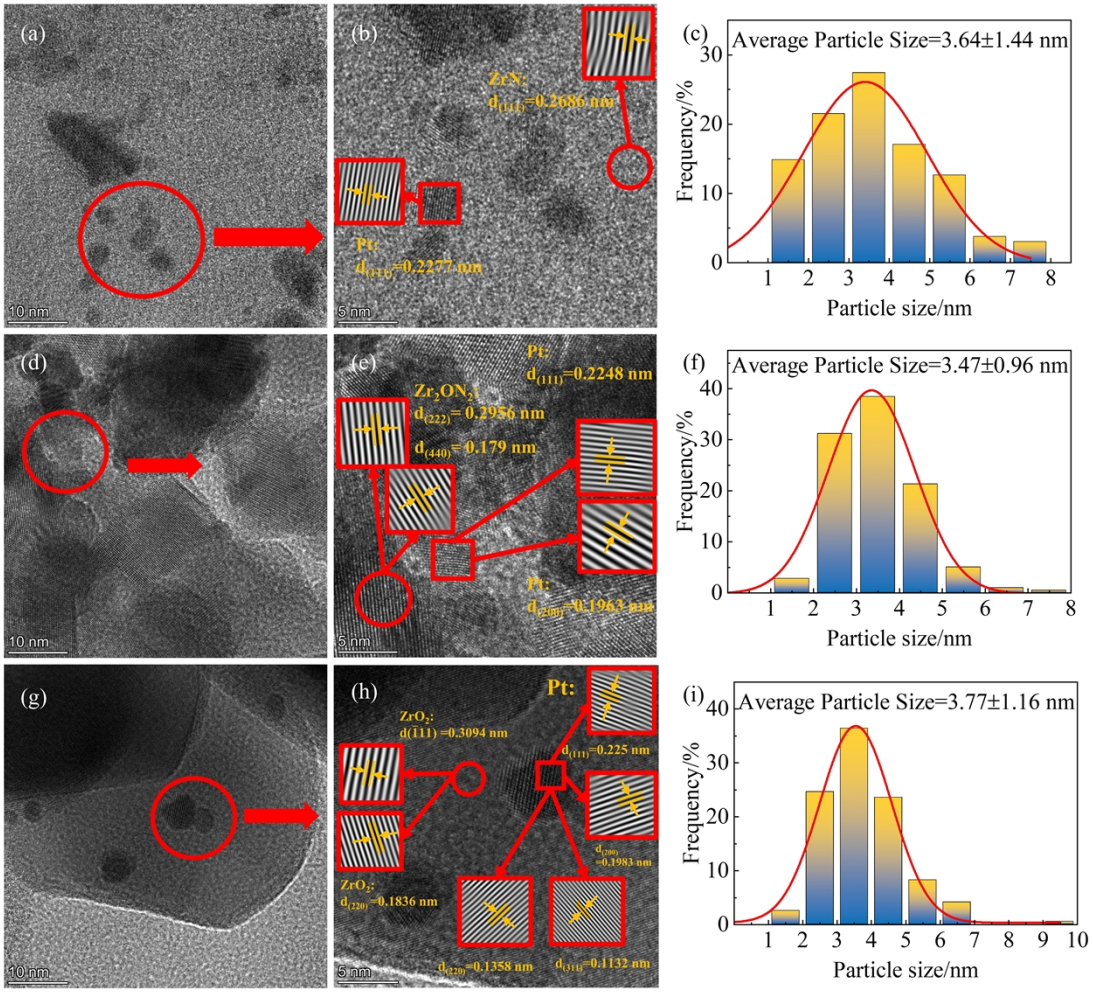

Fig.S3 The TEM images of (a)(b) Pt/ZrN, (d)(e) Pt/Zr_2ON_2, (g)(h) Pt/ZrO_2. (c), (f) and (i) are the corresponding Pt particle size distribution histograms: (c) Pt/ZrN, (f) Pt/Zr_2ON_2 and (i) Pt/ZrO_2.

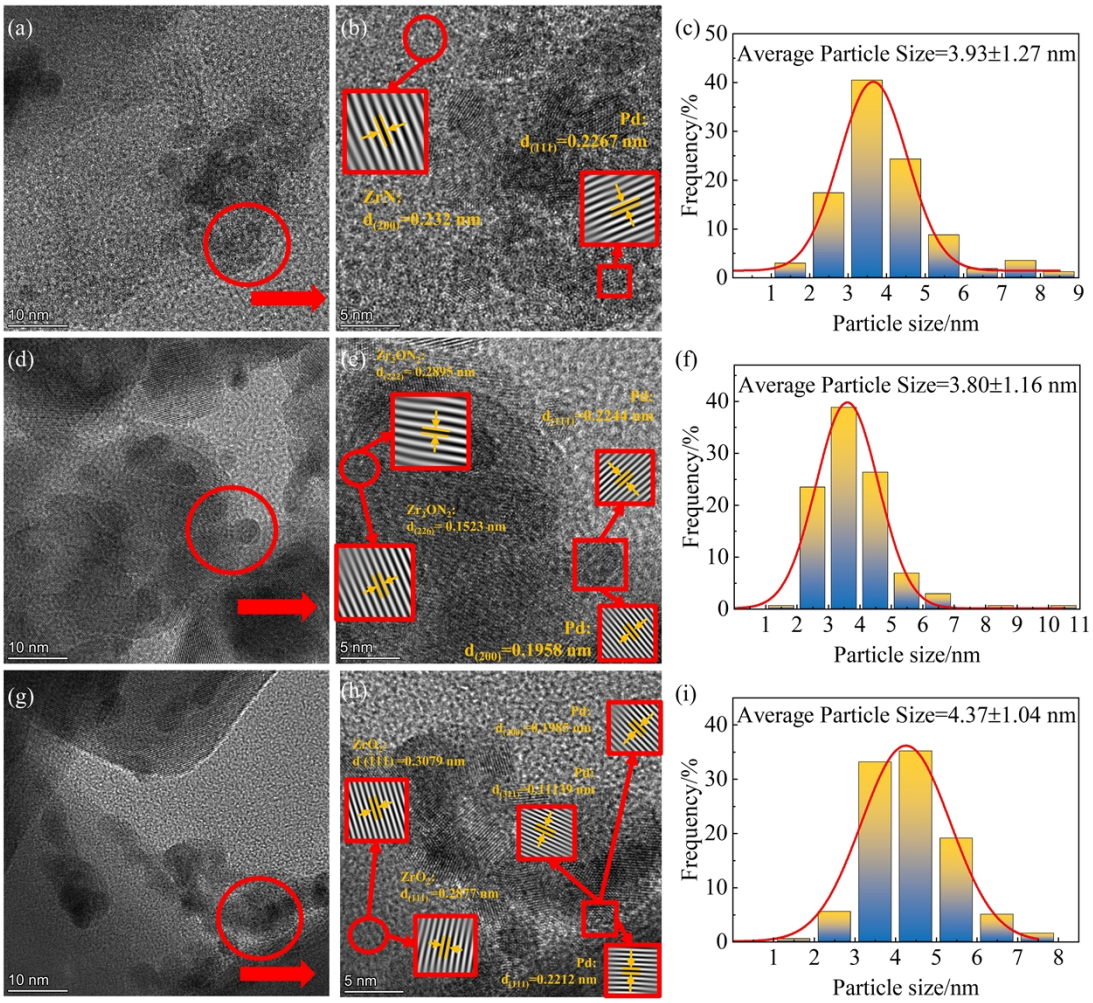

Fig.S4 The TEM images of (a)(b) Pd/ZrN, (d)(e) Pd/Zr_2ON_2, and (g)(h) Pd/ZrO_2. (c), (f) and (i) are the corresponding particle size distribution histograms: (c) Pd/ZrN, (f) Pd/Zr_2ON_2 and (i) Pd/ZrO_2.

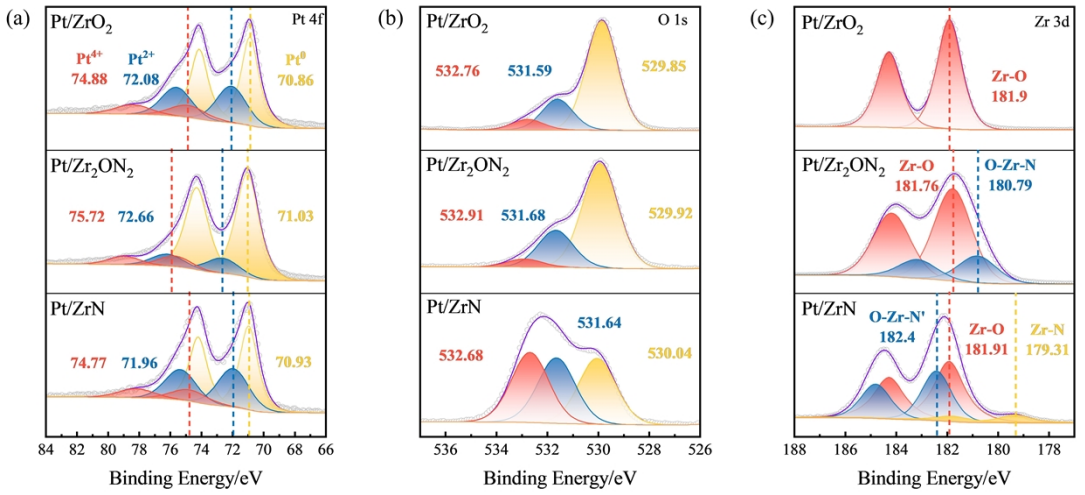

Fig.S5 High-resolution XPS spectra of (a) Pt 4f, (b) O 1s and (c) Zr 3d for Pt-based catalysts (Pt/ZrN, Pt/Zr_2ON_2 and Pt/ZrO_2).

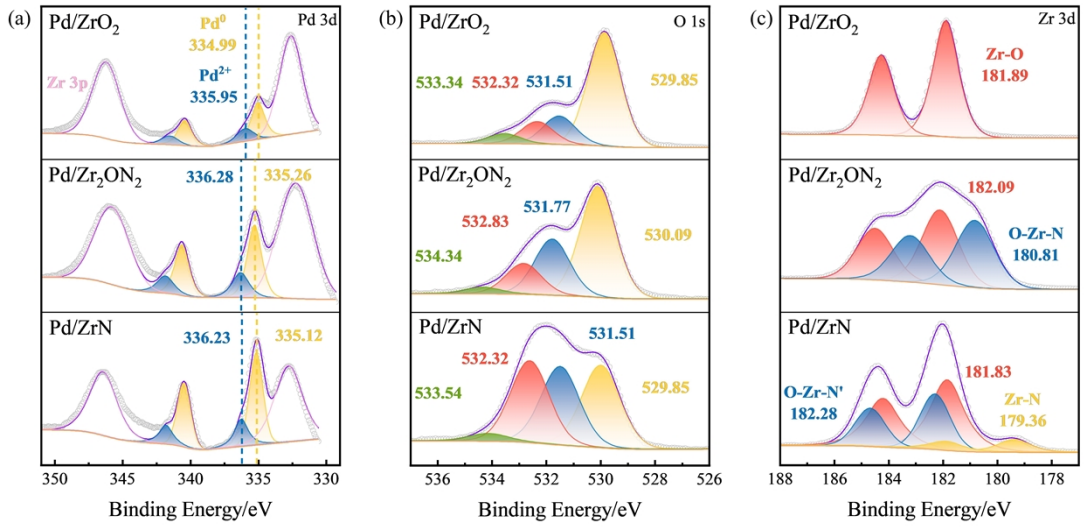

Fig.S6 High-resolution XPS spectra of (a) Pd 3d, (b) O 1s and (c) Zr 3d for Pd-based catalysts (Pd/ZrN, Pd/Zr_2ON_2 and Pd/ZrO_2).

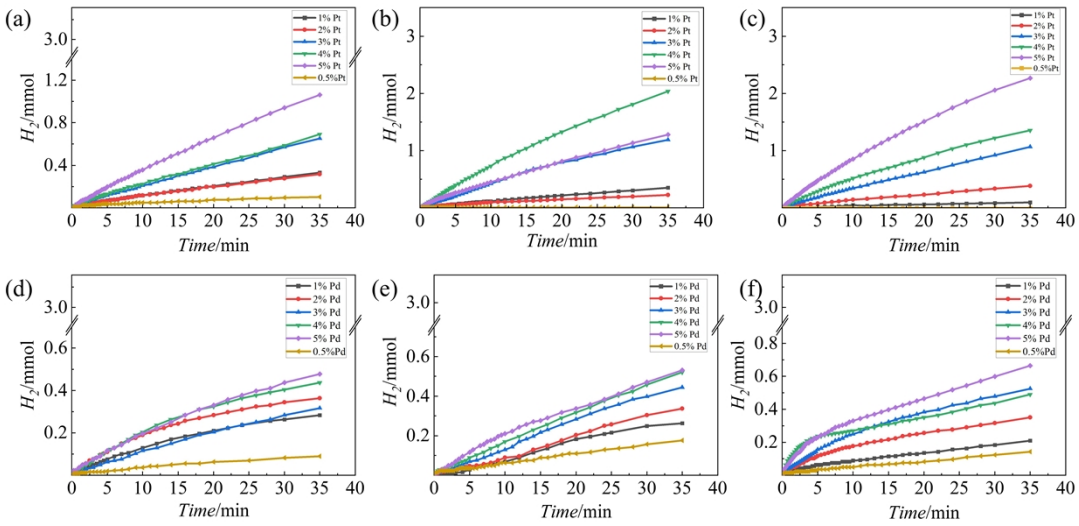

Fig.S7 H_2 evolution profiles from AB hydrolysis for Pt- and Pd-based catalysts with varying metal loadings (0.5-5 wt%). (a-c) H_2 generation vs. time curves for Pt on (a) ZrN, (b) ZrO_2, (c) Zr_2ON_2. (d-f) H_2 generation vs. time curves for Pd on (d) ZrN, (e) ZrO_2 and (f) Zr_2ON_2.

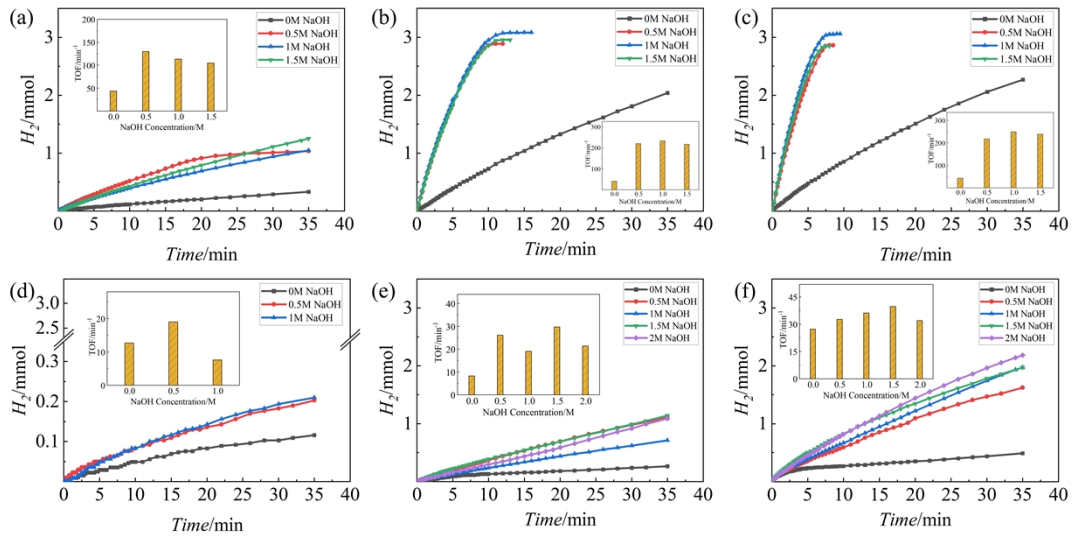

Fig.S8 Influence of NaOH concentration (0-2 M) on the catalytic activity of Pt- and Pd-based catalysts. (a-c) H_2 generation vs. time curves for Pt on (a) ZrN, (b) ZrO_2 and (c) Zr_2ON_2. (d-f) H_2 generation vs. time curves for Pd on (d) ZrN, (e) ZrO_2 and (f) Zr_2ON_2. Inner histograms display the TOF changes with a volcano-shaped trend with optimal activity at 0.5-1 M NaOH.

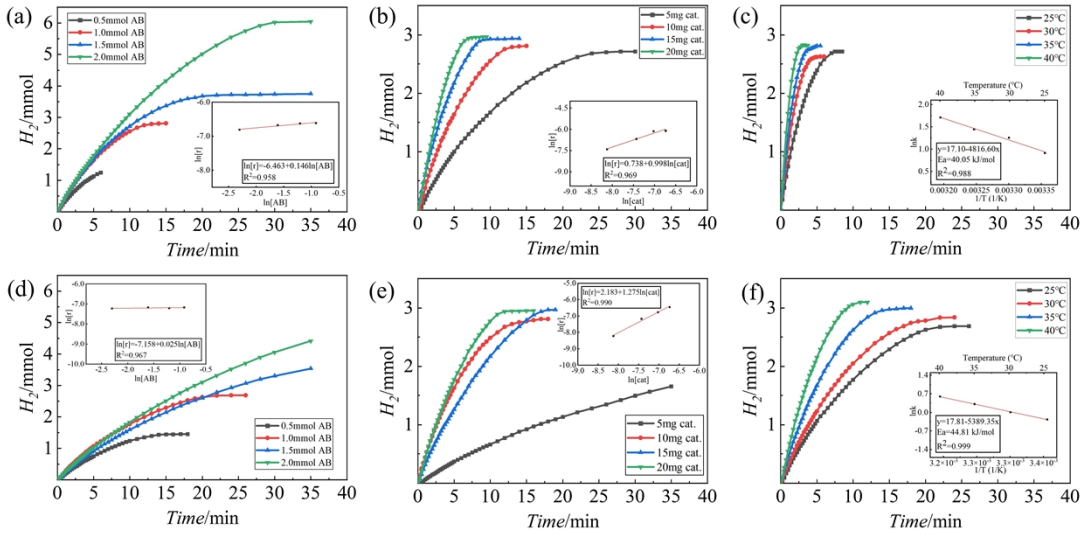

Fig.S9 Kinetic studies of AB hydrolysis over (a-c) Ru/ZrO_2 and (d-f) Ru/Zr_2ON_2. (a)(d) H_2 evolution profiles with varying AB concentration (0.5-2 mmol). Inset shows the logarithmic plot of initial H_2 generation rate vs. [AB], demonstrating zero-order dependence on [AB]; (b)(e) H_2 evolution profiles with varying catalyst dosages (5-20 mg). Inset shows the logarithmic plot of initial H_2 generation rate vs. catalyst dosage, showing first-order dependence on [catalyst]; (c)(f) H_2 evolution profiles with varying temperatures (25-40 °C). Inset shows the Arrhenius plot of initial H_2 generation rate vs. temperature, yielding *Ea* of 40.05 kJ/mol (Ru/ZrO_2) and 44.81 kJ/mol (Ru/Zr_2ON_2).

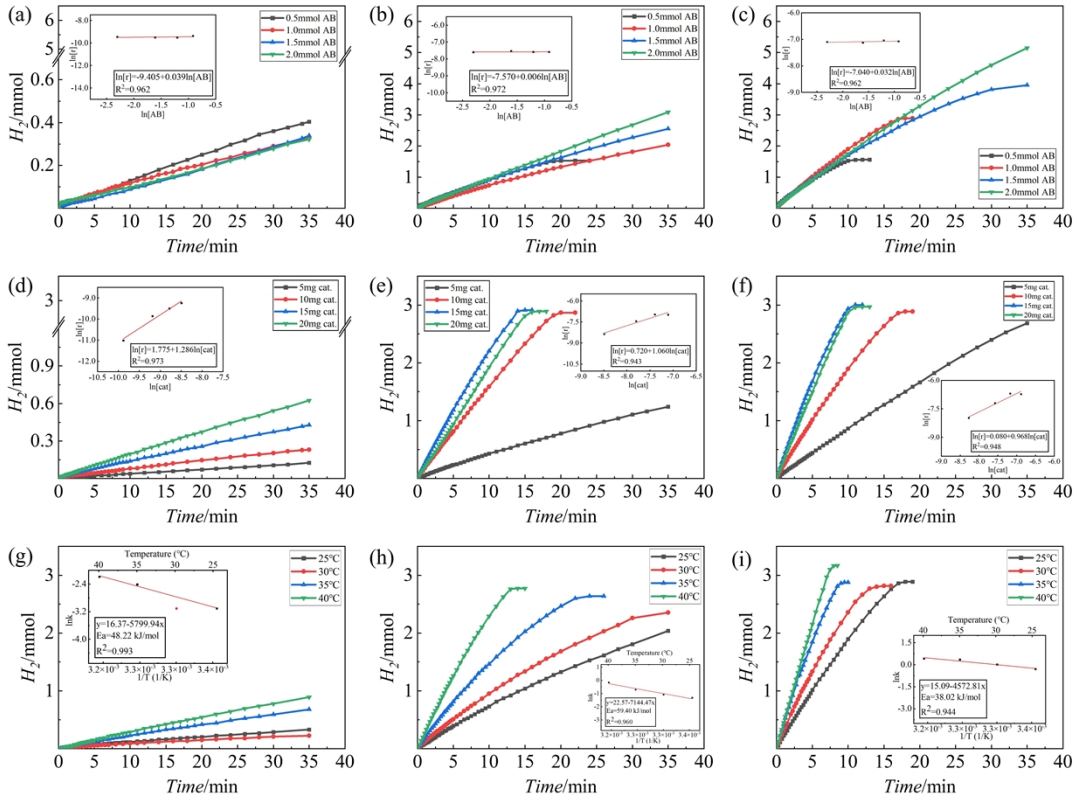

Fig.S10 Kinetic studies of AB hydrolysis over Pt-based catalysts. (a-c) H_2 evolution profiles with varying AB concentration (0.5-2 mmol) on (a) Pt/ZrN, (b) Pt/ZrO_2 and (c) Pt/Zr_2ON_2. Insets show the logarithmic plot of initial H_2 generation rate vs. [AB], demonstrating zero-order dependence on [AB]. (d-f) H_2 evolution profiles with varying catalyst dosages (5-20 mg) on (d) Pt/ZrN, (e) Pt/ZrO_2 and (f) Pt/Zr_2ON_2. Inset shows the logarithmic plot of initial H_2 generation rate vs. catalyst dosage, showing first-order dependence on [catalyst]. (g-i) H_2 evolution profiles with varying temperatures (25-40 ℃) on (g) Pt/ZrN, (h) Pt/ZrO_2 and (i) Pt/Zr_2ON_2. Insets show the Arrhenius plot of initial H_2 generation rate vs. temperature, yielding *Ea* of 48.22 kJ/mol (Pt/ZrN), 59.4 kJ/mol (Pt/ZrO_2) and 38.2 kJ/mol (Pt/Zr_2ON_2).

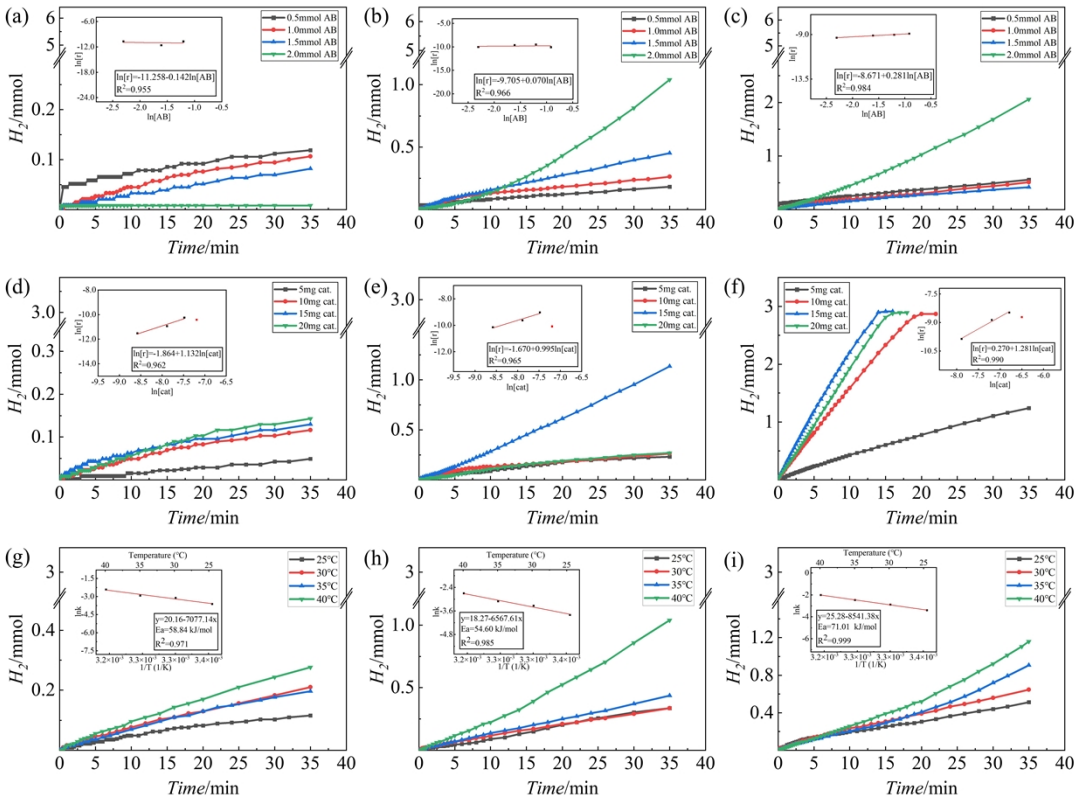

Fig.S11 Kinetic studies of AB hydrolysis over Pd-based catalysts. (a-c) H_2 evolution profiles with varying AB concentration (0.5-2 mmol) on (a) Pd/ZrN, (b) Pd/ZrO_2 and (c) Pd/Zr_2ON_2. Insets show the logarithmic plot of initial H_2 generation rate vs. [AB], demonstrating zero-order dependence on [AB]. (d-f) H_2 evolution profiles with varying catalyst dosages (5-20 mg) on (d) Pd/ZrN, (e) Pd/ZrO_2 and (f) Pd/Zr_2ON_2. Inset shows the logarithmic plot of initial H_2 generation rate vs. catalyst dosage, showing first-order dependence on [catalyst]. (g-i) H_2 evolution profiles with varying temperatures (25-40 °C) on (g) Pd/ZrN, (h) Pd/ZrO_2 and (i) Pd/Zr_2ON_2. Insets show the Arrhenius plot of initial H_2 generation rate vs. temperature, yielding *Ea* of 58.84 kJ/mol (Pd/ZrN), 54.6 kJ/mol (Pd/ZrO_2) and 71.01 kJ/mol (Pd/Zr_2ON_2).

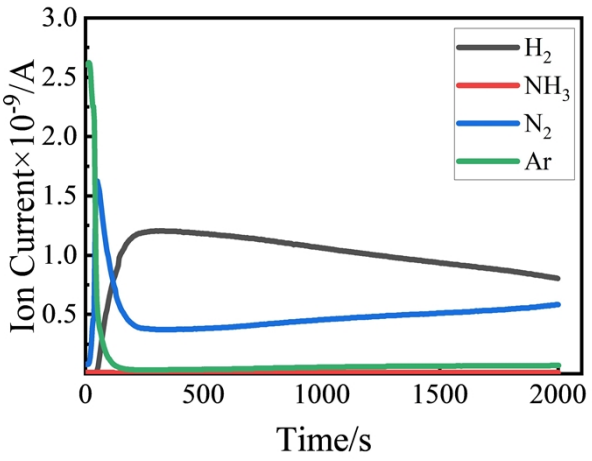

Fig.S12 Online MS graph of gas product collected from AB dehydrogenation catalyzed by Ru/ZrN. (Experimental condition:10 mg catalysts, 1 mmol AB and 5 mL water, water bath, 25 ℃)

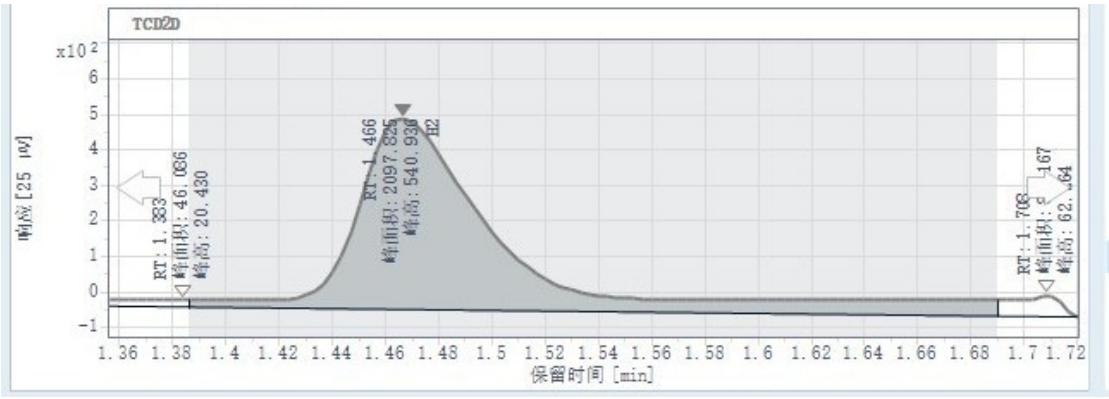

Fig.S13 GC-TCD graph of gas product collected from AB dehydrogenation catalyzed by Ru/ZrN. The retention time of H_2 is 1.47 min. (Experimental condition: 10 mg catalysts, 1 mmol AB and 5 mL water, water bath, 25 ℃)

TableS1 Composition of the synthesized catalyst surfaces calculated from the XPS spectra

Catalyst	$M^0/M^{\delta+}$	Composition (Atomic percent: at. %)				M/Zr	N/Zr
		M	N [1s]	O [1s]	Zr [3d]		
Ru/ZrN	4.40	9.38	4.61	49.56	12.28	0.7638	0.3754
Ru/Zr_2ON_2	2.62	4.36	7.2	45.73	35.53	0.1227	0.2026
Ru/ZrO_2	3.49	5.28	-	43.02	26.36	0.2003	-
Pt/ZrN	1.06	2.42	3.78	46.64	16.49	0.1468	0.2292
Pt/Zr_2ON_2	3.12	4.77	6.07	35.45	31.24	0.1527	0.1943
Pt/ZrO_2	1.23	2.10	-	42.08	30.97	0.0678	-
Pd/ZrN	3.00	2.97	4.01	39.89	15.2	0.1954	0.2638
Pd/Zr_2ON_2	4.32	3.14	6.14	31.5	23.63	0.1329	0.2598
Pd/ZrO_2	2.17	1.86	-	30.76	21.21	0.0877	-

TableS2 Comparison of turnover frequency (TOF) and activation energies (*Ea*) of the high activity catalysts in hydrolytic dehydrogenation of AB at room temperature (298 K)

Catalyst	**Metal/AB (molar ratio)**	**TOF/(min^{-1})**	**Ea/($kJ \cdot mol^{-1}$)**	**Reference**
3%Ru/ZrN	0.003	305.3	31.48	This work
3%Ru/Zr_2ON_2	0.003	147.4	44.81	This work
3%Ru/ZrO_2	0.003	251.2	40.05	This work
Ru/ZrO_2	0.006	173	58	1
Ru/SiO_2	0.0025	200	38.2	2
Ru/TiO_2	0.0012	241	70	3
Ru/Carbon nanotubes	0.0019	329	33	4
Ru/V_O-Co_3O_4	(0.18 wt% Ru)	2114	58.8	5
Ru/g-C_3N_4	0.002	122(303K)	35.6	6
1%Pt/ZrN	0.0005	34.8	48.22	This work
5%Pt/Zr_2ON_2	0.0025	42.7	38.2	This work
4%Pt/ZrO_2	0.002	40.3	59.4	This work
Pt-CeO_2	0.018	182	-	7
Pt-CNT	0.0047	400	38	8
Pt@MIL-101	0.0029	414	41	9
Pt^0/Co_3O_4	0.00025	4366	71	10
Pt@RF	31.03 wt% Pt	176.3	13.69	11
1%Pd/ZrN	0.001	23.8	58.84	This work
4%Pd/Zr_2ON_2	0.004	27.3	71.01	This work
2%Pd/ZrO_2	0.002	8.3	54.6	This work
Pd/CeO_2	0.0011	29	68	12
Pd/ZrO_2	0.0228	3.5	-	12
Pd@MIL-101	0.0189	45	-	13
RGO/Pd	0.0425	6.25	51	14
Pd^0/C-Fe	0.0075	29	-	15
Pd^0/PDA-Fe_3O_4	0.009	14.5	65	16

References:

1. Y. Tonbul, S. Akbayrak and S. Ozkar, *J Colloid Interface Sci*, 2018, **513**, 287–294.
2. Q. Yao, W. Shi, G. Feng, Z.-H. Lu, X. Zhang, D. Tao, D. Kong and X. Chen, *Journal of Power Sources*, 2014, **257**, 293–299.
3. S. Akbayrak, S. Tanyıldızı, İ. Morkan and S. Özkar, *International Journal of Hydrogen Energy*, 2014, **39**, 9628–9637.
4. S. Akbayrak and S. Ozkar, *ACS Appl Mater Interfaces*, 2012, **4**, 6302–6310.

5. X. Zhang, Q. Zhang, Y. Peng, X. Ma and G. Fan, *International Journal of Hydrogen Energy*, 2022, **47**, 7793–7801.
6. Y.-T. Li, S.-H. Zhang, G.-P. Zheng, P. Liu, Z.-K. Peng and X.-C. Zheng, *Applied Catalysis A: General*, 2020, **595**.
7. X. Wang, D. Liu, S. Song and H. Zhang, *Chem Commun (Camb)*, 2012, **48**, 10207–10209.
8. W. Chen, J. Ji, X. Feng, X. Duan, G. Qian, P. Li, X. Zhou, D. Chen and W. Yuan, *J Am Chem Soc*, 2014, **136**, 16736–16739.
9. A. Aijaz, A. Karkamkar, Y. J. Choi, N. Tsumori, E. Ronnebro, T. Autrey, H. Shioyama and Q. Xu, *J Am Chem Soc*, 2012, **134**, 13926–13929.
10. S. Akbayrak and S. Ozkar, *ACS Appl Mater Interfaces*, 2021, **13**, 34341–34348.
11. Y. Dai, W. Zheng, X. Li, B. Chen, L. Wang and G. He, *Chemical Engineering Journal*, 2016, **293**, 252–258.
12. Y. Tonbul, S. Akbayrak and S. Özkar, *International Journal of Hydrogen Energy*, 2016, **41**, 11154–11162.
13. H. Dai, J. Su, K. Hu, W. Luo and G. Cheng, *International Journal of Hydrogen Energy*, 2014, **39**, 4947–4953.
14. P. Xi, F. Chen, G. Xie, C. Ma, H. Liu, C. Shao, J. Wang, Z. Xu, X. Xu and Z. Zeng, *Nanoscale*, 2012, **4**, 5597–5601.
15. S. Akbayrak, G. Çakmak, T. Öztürk and S. Özkar, *International Journal of Hydrogen Energy*, 2021, **46**, 13548–13560.
16. J. Manna, S. Akbayrak and S. Özkar, *RSC Advances*, 2016, **6**, 102035–102042.